Nanotechnology

PAPER

Preliminary studies of ^{68}Ga-NODA-USPION-BBN as a dual-modality contrast agent for use in positron emission tomography/magnetic resonance imaging

To cite this article: Afsaneh Lahooti *et al* 2020 *Nanotechnology* **31** 015102

View the article online for updates and enhancements.

IOP ebooks™

Bringing you innovative digital publishing with leading voices to create your essential collection of books in STEM research.

Start exploring the collection - download the first chapter of every title for free.

This content was downloaded from IP address 18.218.56.169 on 23/10/2019 at 20:27

IOP Publishing Nanotechnology
Nanotechnology 31 (2020) 015102 (11pp) https://doi.org/10.1088/1361-6528/ab4446

Preliminary studies of ^{68}Ga-NODA-USPION-BBN as a dual-modality contrast agent for use in positron emission tomography/magnetic resonance imaging

Afsaneh Lahooti[1,3], **Saeed Shanehsazzadeh**[1] and **Sophie Laurent**[1,2]

[1] NMR and Molecular Imaging Laboratory, Department of General, Organic and Biomedical Chemistry, University of Mons, 23 Place du Parc, B-7000, Mons, Belgium
[2] Center for Microscopy and Molecular Imaging (CMMI), Rue Adrienne Bolland, 8, B-6041 Gosselies, Belgium

E-mail: afsanehlahooti@gmail.com

Received 6 June 2019, revised 17 July 2019
Accepted for publication 13 September 2019
Published 8 October 2019

Abstract

The aim of this study was to propose a new dual-modality nanoprobe for positron emission tomography/magnetic resonance imaging (PET/MRI) for the early diagnosis of breast cancer. For synthesis of the nanoprobe, polyethylene glycol-coated ultra-small superparamagnetic iron-oxide nanoparticles (USPION) armed with NODA-GA chelate and grafted with bombesin (BBN) were radiolabeled with ^{68}Ga. After characterization, *in vitro* studies to evaluate the cell binding affinity of the nanoprobe were done by performing Perl's Prussian blue cell staining and MRI imaging. Finally, for *in vivo* studies, magnetic resonance images were taken in SCID mice bearing breast cancer tumor pre- and post-injection, and a multimodal nanoScan PET/computed tomography was used to perform preclinical imaging of the radiolabeled nanoparticles. Afterwards, a biodistribution study was done on sacrificed mice. The results showed that the highest r_1 and r_2 values were measured for USPIONs at 20 and 60 MHz, respectively. From the *in vitro* studies, the optical density of the cells after incubation increased with the increase of the iron concentration and the duration of incubation. However, the T_2 values decreased when the iron concentration increased. Furthermore, from *in vivo* studies, the T_2 and signal intensity decreased during the elapsed time post-injection in the tumor area. In this study, the *in vitro* studies showed that the affinity of cancer cells to nanoprobe increases meaningfully after conjugation with BBN, and also by increasing the duration of incubation and the iron concentration. Meanwhile, the *in vivo* results confirmed that the blood clearance of the nanoprobe happened during the first 120 min post-injection of the radiolabeled nanoprobe and also confirmed the targeting ability of that to a gastrin-releasing peptide receptor positive tumor.

Supplementary material for this article is available online

Keywords: PET/MRI, iron-oxide nanoparticles, bombesin, molecular imaging

(Some figures may appear in colour only in the online journal)

Introduction

Breast cancer constitutes one of the most common tumor diseases affecting women and ranks second in cancer deaths in women worldwide [1]. Early diagnosis has significantly improved the treatment in recent years [2] with a considerable 5 year increase in relative survival [3]. In order to diagnose breast tumors, strategies such as mammography, x-ray-based computed tomography (CT), magnetic resonance imaging (MRI), bone scintigraphy as well as isotopic imaging

[3] Author to whom any correspondence should be addressed.

 © 2019 IOP Publishing Ltd Printed in the UK

(positron emission tomography (PET) and single photon emission/CT) have been developed [2].

Among the different modalities used in molecular imaging (MI), the combination of PET imaging with MRI, which provides high resolution anatomical information in particular on soft tissue contrast, has introduced a wealth of diagnostic information for numerous clinical applications and may increase the diagnostic accuracy compared to single modalities [4, 5].

The use of an appropriate peptide can lead to improving cancer cells detection *in vivo* which is one of the most challenging issues in MI [6–9]. In the context of using of bombesin (BBN), a 14-amino acid peptide originally isolated from the skin of the European fire-bellied toad (Bombina bombina), constitutes a good candidate for a cancer biomarker since BBN receptors are overexpressed particularly as the gastrin-releasing peptide (GRP) receptor subtype in a number of human tumors, including breast cancer, prostate cancer, small cell lung cancer, ovarian cancers, endometrial cancers, and gastrointestinal stromal tumors [10–13]. In 2015 Jafari *et al* showed that dextran-coated iron-oxide nanoparticles (NPs) labeled with BBN were greatly attached to the breast cancer cell lines [6]. The ability of NPs to act as suitable carriers for *in vivo* drug delivery has been introduced previously [14, 15]. They are used in the recognition, detection, and treatment of cancer [16], and ultra-small superparamagnetic iron-oxide nanoparticles (USPION) have been selected as a carrier of BBN. They present some important characteristics such as bioavailability, non-toxicity, enhanced permeability, and retention effect [17] and high relaxivity which make them as an excellent contrast agent in MRI [18].

The present study aims to propose a new dual-modality nanoprobe for PET/MRI purposes in the early diagnosis of breast cancer. This nanoprobe is based on polyethylene glycol (PEG)-coated USPION conjugated with BBN radiolabeled with a positron emitter, ^{68}Ga, by NODA-GA chelation. ^{68}Ga constitutes a positron-emitting radioisotope suitable for clinical PET applications with a half-life of around 67 min [14]. The targeting efficiency of the nanoprobe was investigated *in vitro* by cell labeling and Prussian blue (PB) staining as well as *in vivo* using MRI and PET/CT images and *ex vivo* via biodistribution studies.

Materials and methods

Materials

(Tyr4,D-Phe^{12})-BBN, high-affinity BBN receptor antagonist based, was purchased from Bachem (Germany). 3-triethoxysilylpropyl succinic anhydride (TEPSA) was purchased from abcr GmbH & Co. KG (Karlsruhe, Germany). $FeCl_3.6H_2O$ (45%) was purchased from Honeywell Riedel-de Haën (Seelze, Germany). Tetramethylammonium hydroxide (TMAOH) (>97%), oleyl alcohol (>60%), and 1, 2-hexadecanediol (>98%) were purchased from TCI (Zwijndrecht, Belgium). Solvents were purchased from Chem-Lab (Zedelgem, Belgium). All other reagents were obtained from Sigma-Aldrich (Bornem, Belgium). ^{68}Ge/^{68}Ga was eluted from a generator Model IGG100 (Eckert & Ziegler, Germany).

Preparation of TEPSA-modified magnetic NPs. Iron-oxide NPs were prepared by co-precipitation of iron salts (ferrous chloride tetrahydrate salt and ferric chloride) in diethyleneglycol at 170 °C under nitrogen atmosphere and under stirring in the presence of sodium hydroxide according to our previous study [19]. TEPSA was then slowly added to the NP dispersion in Dimethylformamide (DMF), and water was then added followed by the addition of an aqueous solution of TMAOH (1 M). The solution was heated at 100 °C for 24 h and the magnetic nanoobjects were collected after pouring the suspension in an acetone/diethyl ether mixture and magnetic decantation.

Synthesis of BBN/NODA/PEG labeled magnetic NPs. A small amount of BBN (1 μmol; 1.6 mg) and NODA-NH_2 (2 μmol; 0.8 mg) was added to an aqueous dispersion of TEPSA-modified NPs (110 mM in iron; 5 ml) in the presence of *N*-(3-dimethylaminopropyl)-*N*′-ethylcarbodiimide hydrochloride (80 μmol; 15.2 mg) as a coupling agent at pH = 7. After one night under stirring, *O*-(2-aminoethyl)-*O*′-methyl PEG (135 μmol; 101 mg) was added to the ferrofluid in the presence of 1-ethyl-3-(3-dimethylaminopropyl)carbodiimide hydrochloride (EDC) (200 μmol; 38 mg). The pH has then been adjusted to 7.5 and the mixture stirred at room temperature. After 15 h of reaction, the suspension was purified by membrane filtration (membrane cut-off = 30 kDa) and finally centrifuged (16 500 G; 40 min).

Radiolabeling of NODA-USPIONs-BBN with ^{68}Ga and determination of labeling yields.. PEG-coated USPIONs armed with an NODA-GA chelator and grafted with BBN were radiolabeled with ^{68}Ga. To this aim ^{68}Ge/^{68}Ga generator was eluted with suprapure HCl (0.1 M, 10 ml) in 0.5 ml fractions. The labeling process was performed using 5 different buffers and pHs. 1 M acetate buffer with a range of different pH (4, 4.5, 5, and 5.5, respectively), and 0.6 M of 4-(2-hydroxyethyl)-1-piperazineethanesulfonic acid (HEPES) buffer were used. The samples were kept at room temperature for 30 min

Instant thin layer chromatography (ITLC) was used to determine the radioactive labeling yield. The following mobile phases were used: pyridine/acetic acid/H_2O (ratio of 3/5/1.5) and saline. The ITLC paper was used as the solid phase.

The labeling efficiency was obtained as follows (1):

$$\text{Labeling efficiency}\% = \frac{\text{Total counts} - \text{counts of free } ^{68}\text{Ga}}{\text{Total counts}} \times 100. \quad (1)$$

Characterization of PEG-coated USPIONPs. The size and morphology of the NPs were examined by using a transmission electron microscope (TEM; Tecnai 10(80 kV), FEI Company, USA). For TEM investigation, the NPs were deposited on a copper-grid-supported perforated transparent

carbon coil. The measurements of the hydrodynamic diameters of the NPs were performed by photon correlation spectroscopy using a Zeta-sizer Nano Series Zen 3600 (Malvern, Worcestershire, United Kingdom) at 25 °C before and after conjugation with BBN as well as after radiolabeling. The transverse and longitudinal relaxivities (r_1 and r_2) of the NPs before and after conjugation were assessed at room temperature with Bruker Minispec systems mq-20 and mq-60 (Bruker, Karlsruhe, Germany) in two different frequencies (20 and 60 MHz). Finally, the iron concentration of NPs was determined by relaxometry after digestion of NPs using a microwave digestion system.

In vitro study

Two breast cancer cell lines were derived, MDA-MB-231 and MCF-7, which express gastrin-releasing peptide receptor (GRPR; BBN binds with high affinity to the GRPR), and were used as the model. Cells were cultured in Dulbecco's Modified Eagle Medium media, high glucose plus fetal bovine serum to 10%, and glutamine to 2 mM.

To evaluate the ability of the cells to bind the particle, the MDA-MB-231 and MCF-7 cell lines were incubated with NPs couples with or without BBN at different concentrations and different time points. Cell binding affinity was performed using Perl's PB cell staining that allows the visualization of the iron within cells and MRI T_2 measurement.

PB cell staining assay was performed as follows. Cells were cultured on cover slips overnight and then fixed with 37% formaldehyde before incubation with the nanoprobe (100 and 200 mg ml^{-1} concentration for 30, 60, and 120 min). The cells were then washed with phosphate buffered saline (PBS) and incubated for 30 min with 5% potassium ferric-ferrocyanide (Perl's PB reagent for staining; Sigma-Aldrich) in 2% hydrochloric acid. After incubation of the cells with 3,3′-Diaminobenzidine and Luxol blue solution, for 10 min and 30 s, respectively, the samples were washed with ethanol. The evaluation of iron staining was performed using light microscopy (Leica DM2500, Leica Microsystems GmbH, Wetzlar, Germany). The images were quantified with Fiji software (ImageJ distribution, USA) to plot the optical density measured.

The affinity of MDA-MB-231 cells to conjugated NPs with BBN was evaluated by MRI after incubation with a nanoprobe. In practice, the 3×10^5 cells/well were cultured on a six-well plate with 2 ml of culture medium. On the day of the experiment, the cells were incubated with four different concentrations of NODA-USPION-BBN (200, 100, 50, and 10 μg ml^{-1}), NODA-USPION (200 μg ml^{-1}) and PBS for 120 min at room temperature after washing with PBS. After incubation, they were trypsinized and fixed in 2% gelatin microtubes. The samples were then scanned and T_2-weighted images were acquired with a spin-echo imaging sequence using a 9.4 T horizontal bore small animal MR scanner imaging system (Bruker Biospec, Germany). The imaging parameters were as follows: repetition time, 3000 ms; echo time, from 15–960 ms with 15 ms intervals; field of view (FoV; 250 × 250 mm; matrix size, 256 × 256; and slice thickness, 3 mm. The data from the regions of interest (ROIs) were drawn to consistently measure the mean signal intensity at the identical position within each phantom vial.

In vivo studies

Mice. Six week old female SCID mice (Charles Rivers Laboratories, L'arbresle, France) were housed in a sterile environment and allowed to acclimatize for 1 week. They were injected by subcutaneous injection of MDA-MB-231 (1×10^6 cells/mouse) in 0.2 ml of a mixture of PBS and Matrigel 1:1 v/v to the right flank. All *in vivo* experiments were carried out in accordance with Ethical Projects CMMI-2011-07 approved by the local Ethical Committee.

MRI. MRI was performed on a 9.4 T Biospec (Bruker, Ettlingen, Germany) using a volume coil (38 mm diameter). The slice thickness was 0.4 mm using a rapid imaging with refocused echoes (RARE) sequence. The parameters for T_2-weighted images were: repetition time = 2000 ms and echo time = 72 ms, MTX = 192 × 96, FoV = 32 × 16 mm, and textural analysis (TA) = 25 min and 36 s.

In accordance with the ethical protocol of the Center for Microscopy and Molecular Imaging (Gosselies, Belgium). These MR images were taken of SCID mice bearing breast cancer tumor pre- and post-nanoprobe tail vein injection. Also all animals were kept anesthetized with 1%–1.5% isoflurane in 100% oxygen (0.4 l min^{-1}) using a mouse nosecone. The respiratory rate was monitored during the entire imaging session and their body temperature was monitored and maintained as well.

PET/CT. A multimodal nanoScan PET/CT (Mediso, Hungary) was used to perform preclinical imaging of the radiolabeled NPs. In practice, 1.1MBq of ^{68}Ga-NODA-USPION-BBN is injected via the tail vein and the mouse is kept anesthetized by gaseous isoflurane during the whole imaging process (3.5% isoflurane for induction; 2% isoflurane for maintenance). Then, the mouse were layed in the camera in a feet-first prone position. Firstly, a CT acquisition was performed on the whole body (50 kV, 520 μA, 480 projections, 300 ms/projection, binning 1:4). The CT reconstruction was performed in parallel of the acquisition with default parameters (medium-medium mode with a cosine filter to provide images with 251 μm size voxels). A 120 min dynamic PET acquisition was then performed starting from the injection of the nanoprobe, with the energy window ranging from 400–600 keV and 1-to-3 detector block coincidence mode. The PET images acquired during the time ranges of 0–2 min, 10–20, 30–40, 50–60, and 115–120 min were reconstructed with an OSEM-3D iterative algorithm (6 iterations, 4 subsets) in normal mode, full detector model, spike filter on, normal regularization mode, and including random scatter and attenuation correction to get images 400 μm in voxel size.

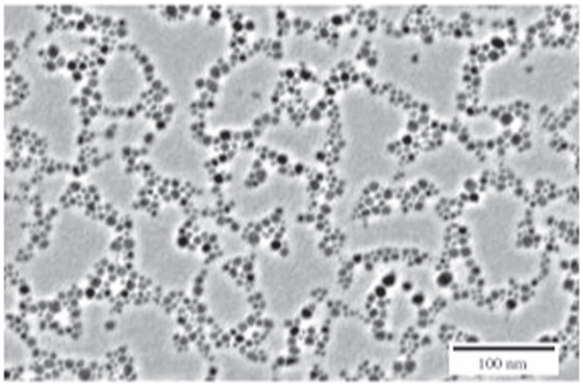

Figure 1. TEM images of synthesized USPION. Mean diameter of the NPs was 7.4 ± 2.3 nm.

PET and CT images were analyzed with VivoQuant software v2.5 (Invicro, USA).

Biodistribution study. Following PET/CT imaging the mice were sacrificed, and organs (liver, spleen, lung, kidney, blood, and urine) were recovered to determine the biodistribution of the radiolabeled NPs. Three mice were sacrificed after the specified time intervals (60, 90, and 120 min post-injection). The activity of each organ was calculated as a percentage of the injected dose per gram tissue (ID/g %) by the Automatic Gamma Counter Wizard2 2480 (Perkin Elmer, USA).

Statistical analysis. Data have been represented as the mean of at least four individual observations with a standard error of mean. The significance has been calculated using the Student's *t*-test.

Results

Characterization of the nanoprobe

Size measurement of the nanoprobes. NP size and morphology were evaluated by TEM (figure 1). The mean particle size of USPION measured is 7.42 ± 2.34 nm.

The hydrodynamic diameter measurements obtained by dynamic light scattering were 20, 22, and 24 nm for USPION, USPION-PEG, and NODA-USPION-BBN respectively. Synthesized USPIONs had a very narrow size distribution allowing for a very uniform biophysicochemical property which is also suitable for drug delivery applications [1].

USPION-PEG-coated and NODA-USPION-BBN present zeta potential values of −30.3 ± 1.8 and −12.6 ± 0.6 mV, respectively, at pH = 5.0.

r_1 and r_2 measurements. The amounts of transverse and longitudinal relaxivities (r_1 and r_2) of the NPs before and after conjugation were obtained using Bruker Minispec systems at two different frequencies (20 and 60 MHz). As shown in table 1, the relaxivities of the NPs decrease after BBN conjugation. These results strongly support the influence of the conjugation in the r_1 and r_2 relaxivity measurements. These results also indicate that the r_1 values decrease as the frequency increases from 20–60 MHz. The highest r_1 value measured is for USPION at 20 MHz frequency and the highest r_2 value is related to USPION at 60 MHz as well.

In vitro study

Cell binding affinity of the nanoprobe. The nanoprobe affinity for GRPR-expressing cells was confirmed by Perl's PB staining and MR imaging techniques. To this aim, GRPR-expressing MDA-MB-231 cells were incubated with NODA-USPION and NODA-USPION-BBN at different concentrations of iron. The MR imaging results are displayed in figure 2(A). The signal intensity of the nanoprobes with iron concentrations of 10, 50, 100, and 200 μg ml^{-1} appears to decrease from 2.935×10^6 to 2.729×10^6. However, the T_2 values decrease when the iron concentration increases (figure 2(B)). Interestingly, the significant difference of signal intensity between the nanoprobe and NODA-USPION (2.729×10^6 and 2.869×10^6, respectively which means an increase of about 1.40×10^5 units in signal intensity) was detected at 200 μg ml^{-1} iron concentration.

PB staining was then performed in order to evaluate the cell binding affinity on the MDA-MB-231 and MCF-7 cell lines incubated with PBS versus NODA-USPION-BBN during 30, 60, and 120 min. The intensity of the brown color confirmed the presence of iron taken by the cells, and increases significantly when the duration of the incubation rises (figure 3).

The optical density measurement of the cells after incubation with NODA-USPION-BBN and USPION-PEG showed a considerable increased in Fe uptake in GRPR-expressing MDA-MB-231 cells when the iron concentration in the medium and duration of the incubation increased (figures 4(a)–(c)).

To confirm that the presence of GRP receptors significantly influences MCF-7 cell uptake of the nanoprobe, a PB staining test was performed on a GRPR-positive MCF-7 cell line incubated with different concentrations of nanoprobe. (The results are shown in figure 1S in the supplementary materials which are available online at stacks.iop.org/NANO/31/015102/mmedia).

In vivo studies

MRI. The mean values of T_2 amounts pre- and post-injection (axial view) were obtained from different regions of interest (ROIs) as indicated in the T_2 map images (figure 5) and summarized in table 2. As expected the T_2 as well as the signal intensity associated decreases during the elapsed time post-injection in the tumor area, and the mean T_2 changes in the tumor appear to be −25.57%. These results confirm the

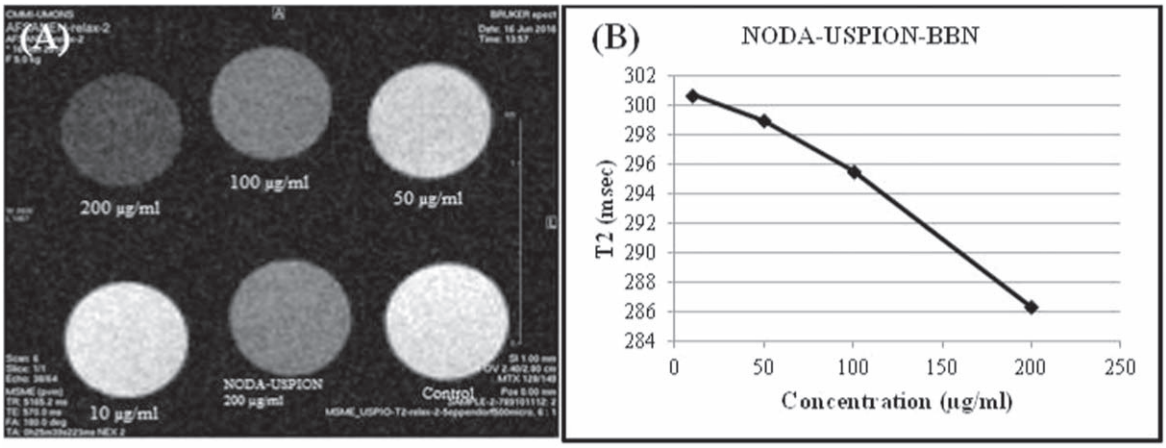

Figure 2. (A) T_2-weighted imaging of MDA-MB-231 cells after 2 h of incubation with different concentrations of NODA-USPION-BBN. NODA-USPION and PBS are shown as controls. (B) Differences in T_2 amounts of cells incubated with NODA-USPION-BBN versus different iron concentrations.

Table 1. r_1 and r_2 values of USPION and NODA-USPION-BBN at 20 and 60 MHz.

Nanoprobe	20 MHz r_1 ($mM^{-1}s^{-1}$)	20 MHz r_2 ($mM^{-1}s^{-1}$)	60 MHz r_1 ($mM^{-1}s^{-1}$)	60 MHz r_2 ($mM^{-1}s^{-1}$)
USPION	36.2	98.1	15.3	110.0
NODA-USPION-BBN	14.7	33.7	6.2	35.4

targeting ability of the nanoprobe to target a GRPR-positive tumor.

PET/CT imaging of the ^{68}Ga-NODA-USPION-BBN

The PET imaging of the mice injected with the ^{68}Ga-NODA-USPION-BBN was performed during 2 h and started exactly at the time of injection. Reconstruction of different time ranges was performed to get the ability to follow the radiotracer biodistribution at early and later stages post-injection (0–2, 10–20, 30–40, 50–60, and 115–120 min).

Snapshots generated from the PET images obtained are shown in figure 6(a). A qualitative analysis of the images suggests that the radioactivity diffuses within the body during the first 2 min post-injection and starts to localize in the liver later on to accumulate finally in the bladder as well as expected since the radiotracer is naturally removed from the body via the urinary tract. As shown in figure 6 as well, tumor uptake is detectable at 120 min post-injection but not yet after 60 min post-injection of the nanoprobe. The mean %ID extracted from the PET/CT images in the tumor area 2 h post-injection was 2.6.

Ex vivo biodistribution studies.. The three rats taken into consideration were dissected at three different time points (one time point for each rat: 60, 90, and 120 min post-injection) to evaluate the biodistribution of the radiolabeled NODA-USPION-BBN *ex vivo*. The results expressed in percentage of radioactivity were measured per organ and corrected for decay compared to the injected dose per rat and normalized per gram (%ID/g) are presented in table 3. As shown in table 3, the uptake of the radioactivity within the different organs of interest, except the liver, decreases gradually with the time.

The clearance of the radiolabeled nanoprobe from the blood was also monitored with time. To this aim different blood punctions were taken at 1, 15, 30, 60, 90, and 120 min post-injection. The results are presented in figure 7. As expected the %ID/g of blood appeared to decrease slowly with time, which confirms that the blood clearance of the nanoprobe happens during the first 120 min post-injection of the radiolabeled nanoprobe.

Discussion

In the field of MI, each approach presents pros and cons in terms of resolution, sensitivity, functional metabolic parameters measurable, and anatomical features. In the context of the improvement of diagnostic accuracy and to provide greater insight into underlying disease processes, PET/MRI constitutes a very promising approach since it combines the benefit of both MR (high spatial resolution) and PET (high sensitivity and measurement of parameters related to metabolism) imaging modalities together. By manipulating magnetic NPs, not only did we increase the tumor uptake as time passed (as demonstrated in figure 6(F)), but we also had a chance to increase the tumor contrast in the MRI images [16, 20–22]. In this study, a dual-modality probe based on magnetic iron-oxide NPs was developed to target tumor cells

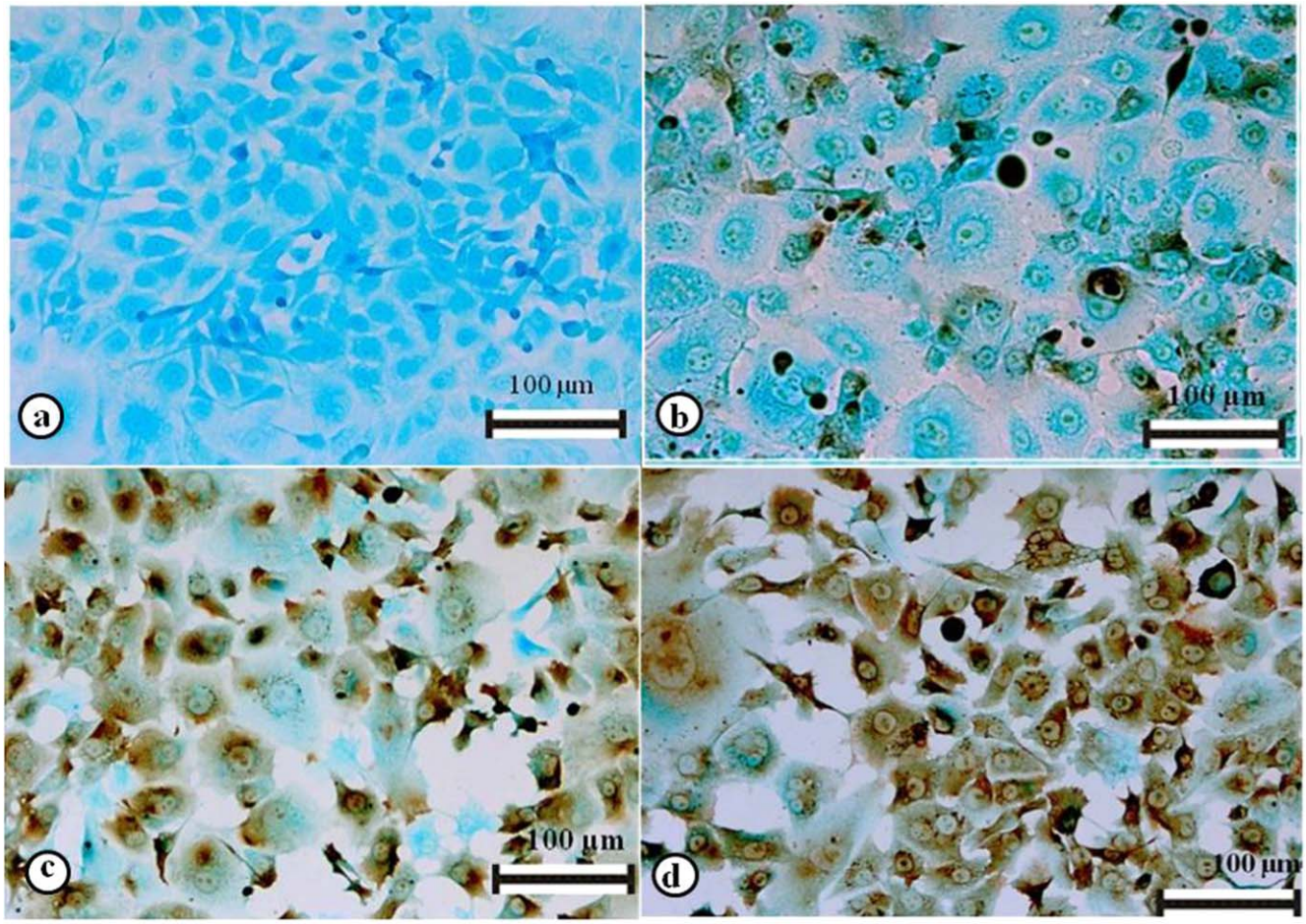

Figure 3. Perl's PB staining images of MDA-MB-231 cell line incubated with either PBS (a) or NODA-USPION-BBN 200 μg ml^{-1} after (b) 30 min, (c) 60 min, and (d) 120 min.

expressing GRPR. In that regard, the BBN peptide was used as a vector to deliver the ^{68}Ga-radiolabeled NPs into certain tumors. Investigations were performed to check the ability of the probe, ^{68}Ga-NODA-USPION-BBN, to target GRPR-expressing tumor cells *in vitro* and *in vivo* using a subcutaneous tumor model and therefore to constitute a dual PET-MR probe usable on patients.

Jafari *et al* in 2015 incubated a dextran-coated SPION–BBN complex with breast cancer cell lines for the same duration, and the cells with the overexpressed GRP receptor on their surface were labeled with targeted NPs [6]. Their results in agreement with ours showing that the selective binding of BBN-conjugated NPs in contrast with non-targeted NPs. In another study, it was demonstrated that there is some uptake of non-targeted gold-NPs in prostate cancer cells which can be related to passive uptake, because of the particles' nanometric size. However, after their conjugation with BBN, the particular tumor cell binding was increased [23] in agreement with another publication [24].

In 2013, Varasteh *et al* published their biodistribution results 1 and 2 h post-injection of ^{68}Ga-NOTA-P2-RM26 (^{68}Ga-labeled NOTA-PEG2[D-Phe^{6},Sta^{13},Leu^{14}] BBN [6 − 14]) in mice. They showed a significant time-dependant reduction in uptake in the blood, spleen, lung, and kidney for the^{68}Ga-labeled conjugate [25]. These data are also in good agreement with our findings and other publications [14, 26, 27]. Moreover, they demonstrated a negligible change in liver uptake after 2 h as we showed after the same time [25].

Previous studies showed that the use of dextran-coated NPs *in vivo* presents a high risk in terms of activation of the immune system since they accumulate in liver and spleen via the absorption of the opsonin-based proteins at the surface of nanoprobes *in vivo* [28–31]. Moreover, some studies have shown that dextran-coated NPs present high reticuloendothelial system (RES) uptakes, up to 80% of %ID/g by the liver and spleen [32–34]. Beside this high RES uptake, there is also the possibility that the biomarker is covered by plasma proteins and reduce therefore the ability of the dextran-coated NPs to target the protein [35–37]. Finally, in contrast to our *in vitro* results, the *in vivo* experiments were not promising, since we noticed high urine uptake of the probe. Although after 2 h post-injection, there was still about 30% of activity in blood but the high volume of urine was not desirable. There are several reasons to justify that phenomenon such as the small size of the NPs as well as *in vivo* instability of the probe and protein corona. As shown in the supplementary materials (figures 2S–4S), our dynamic light

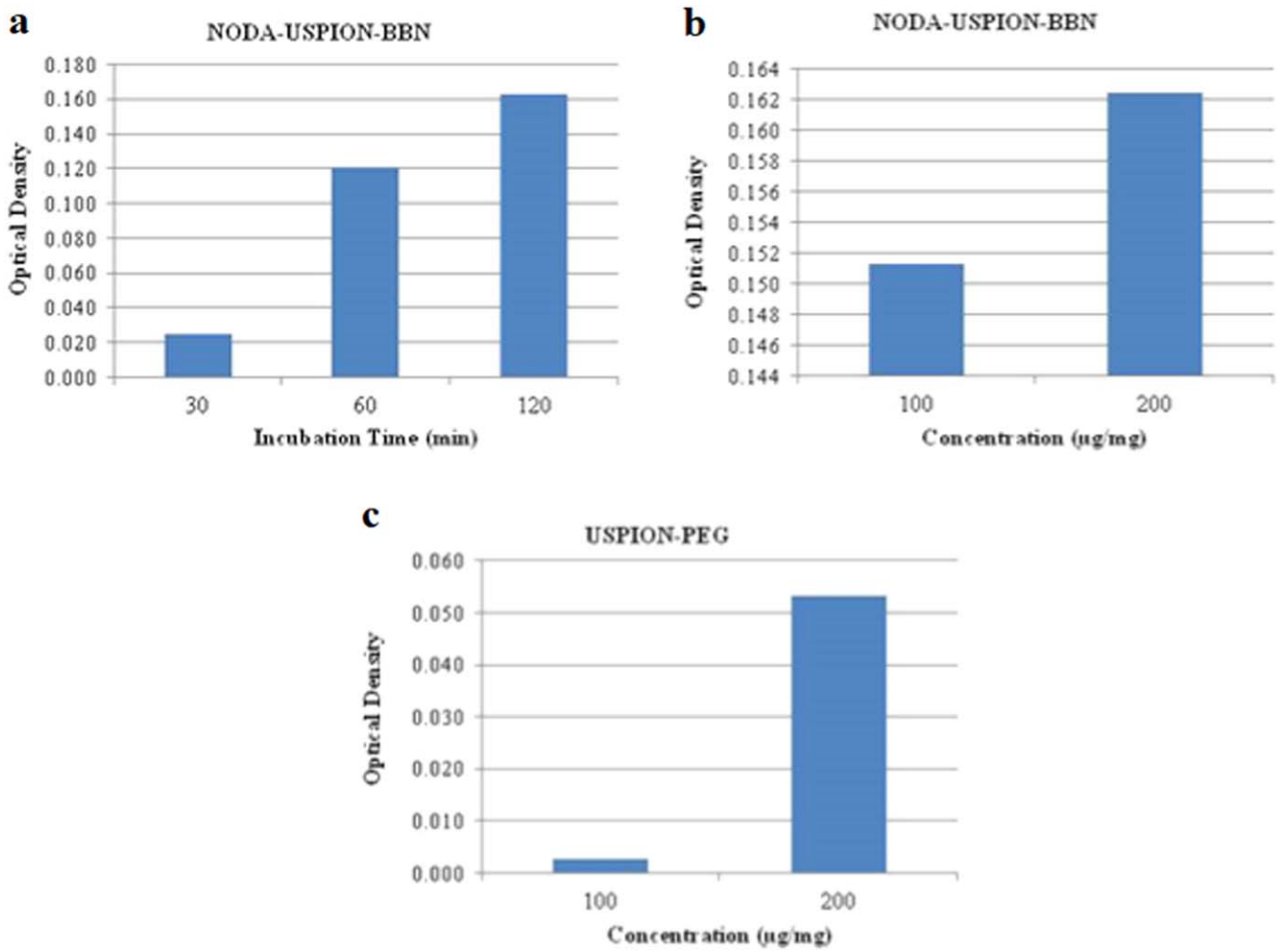

Figure 4. Optical densities of MDA-MB-231 cells incubated with NODA-USPION-BBN; (a) in 200 μg ml^{-1} iron concentration at different time points; (b) in 100 and 200 μg mg^{-1} concentrations during 120 min; (c) with USPION-PEG in 100 and 200 μg ml^{-1} concentrations during 120 min. They were calculated by Fiji software.

scattering (DLS) results showed that the average hydrodynamic sizes were 20, 22, and 24 nm for USPION, USPIONs-PEG, and NODA-USPION-BBN, respectively. Since those are average size and we did not filter the small particles, we had some NPs that were smaller than 20 nm which caused a short blood half-life and high urine uptake in this study. On the other hand, our probe showed high stability at room temperature while we kept it in PBS (as depicted in figure 5S supplementary materials) whereas being in biological milieu, it could have different behavior, but since we used NODA as the chelator agent can reduce the risk of *in vivo* instability. The other important factor could be protein corona. It was suggested that the protein corona could cover the targeted site, leading to a significant reduction in *in vivo* targeting capability [35]. In terms of tumor uptake, Sun *et al* [38] used a different BBN analog (JMV594) labeled with ^{68}Ga with NODA-GA as a chelator and studied its biodistribution in mice bearing prostate cancer. It showed 3.78 $\pm$ 0.28%ID/g 2 h post-injection in comparison with 2.6%ID/g at the same time post-injection of our compound. This difference could be as a result of conjugation of iron-oxide NP to our probe.

Challenges

The first challenge of this study was changing the size of the NPs pre- and post conjugation as well as their size after radiolabeling. It appeared that their hydrodynamic size varies from 19–21 nm before and after conjugation. This slight increase in hydrodynamic size is in accordance with previous studies [27, 39, 40]. Regarding the zeta potential of the NPs after conjugation NPs with chelator and BBN, the surface charge became more positive because of amine groups. In drug delivery, the net charge of injected NPs would be better to be negative in order to increase the targeting efficiency, because the negative charge helps the escape from the RES [41]. However, after getting in touch with the targeted cell membrane, the charge of the NPs will be changed to positive due to interactions with the membrane and its local environment [1].

After conjugation of the peptide, the magnetic properties of the NPs change significantly as shown in table 1 and both their longitudinal and axial relaxivity were decreased. These observations are not only the consequence of the size increments due to the presence of the peptide and chelator [42] but

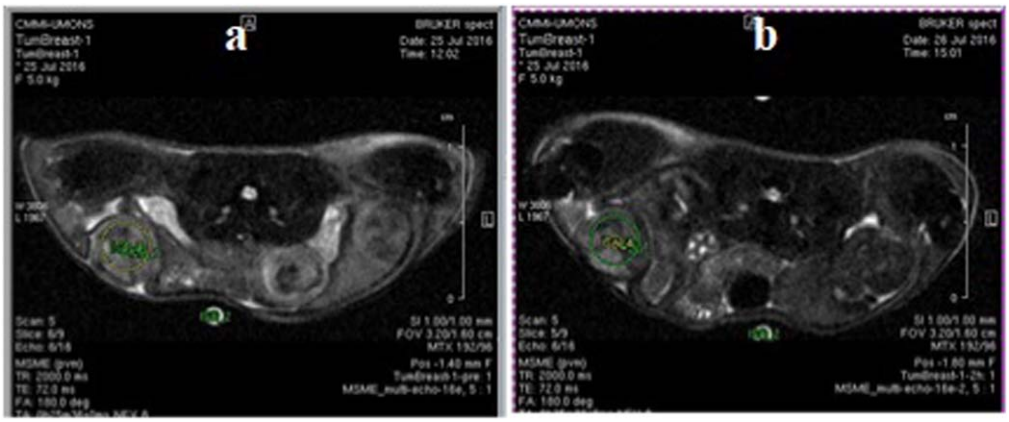

Figure 5. T_2 map image before (a) injection and (b) 2:30 h post-injection of the radiolabeled NPs.

Table 2. T_2 amounts calculated from different ROIs in tumor and muscle derived from the T_2 map images.

Region	T_2 (msec) before Injection	T_2 (msec) 2:30 h Post-injection	Percentage variation of T_2
ROI 4 in muscle	24.2 ± 2.1	24.7 ± 2.18	2.1
ROI 1 in tumor	43.4 ± 2.3	37.3 ± 2.4	−14.1
ROI 2 in tumor	41.5 ± 3.7	26.9 ± 3.1	−35.2
ROI 3 in tumor	42.1 ± 3.7	33.0 ± 3.5	−21.6
ROI 5 in tumor	38.2 ± 3.2	26.2 ± 3.9	−31.4

also because of the changes in their angular momentum and their molecular weights [43]. These data are in accordance with previous studies carried out by others [27, 44] who have reported that after modification and particularly after the addition of some amino acids, the magnetic properties were significantly decreased. It has also been reported that the addition of arginylglycylaspartic acid (RGD) to NPs induce modification of r_2 values at 3 T (151.9 and 105.5 mM^{-1} s^{-1} for NPs and NPs-RGD, respectively) [21]. Due to the higher molecular weights of BBN (about five times higher than RGD), higher changes in r_1 and r_2 were expected and as shown in table 1 this hypothesis was confirmed: conjugation of the peptide to the NPs does induce 68% decrements in r_2 value at 1.5 T compared to unconjugated NPs.

Another limitation that we faced during this study was that we were not able to take MRI images after 2.5 h post-injection. Therefore further studies are still needed. Based on the data collected from PET images, we expected to have higher signal changes after 4 h post-injection. An increase in the tumor uptake as time goes by has been seen. Therefore, later images are recommended.

Conclusion

In this study, a dual-modality probe, ^{68}Ga-NODA-USPION-BBN, was developed to target breast cancer tumor cells and then the ability of the probe to target the GRPR-expressing tumor cells was investigated using *in vitro* and *in vivo* studies. The influence of the conjugation in the r_1 and r_2 relaxivity measurements was supported by the obtained results and also indicated that the r_1 values decrease as frequency increases from 20–60 MHz. The surface charge of the NPs after conjugation with the chelator and BBN became more positive because of amine groups, although it would be better if the net charge of the injected NPs was negative in order to increase the targeting efficiency. *In vitro* studies showed that the affinity of cancer cells to the nanoprobe increases meaningfully after conjugation with BBN, and also by increasing the duration of incubation and iron concentration. Meanwhile, the *in vivo* results confirmed that the blood clearance of the nanoprobe during the first 120 min post-injection of the radiolabeled nanoprobe. In addition, the PET/CT images showed that tumor uptake is detectable at 120 min post-injection. Lastly, from the MRI images, the mean T_2 changes in tumor appeared to be −25.57% which confirms the ability of the nanoprobe to target GRPR-positive tumors.

Acknowledgments

We thank Dimitri Stanicki, Sébastien Boutry, Gilles Doumont, Carmen Burtea, Simon Lacroix, and Serge Goldman for their contribution and Prof. Robert N. Muller for his support.

Conflict of interest

None.

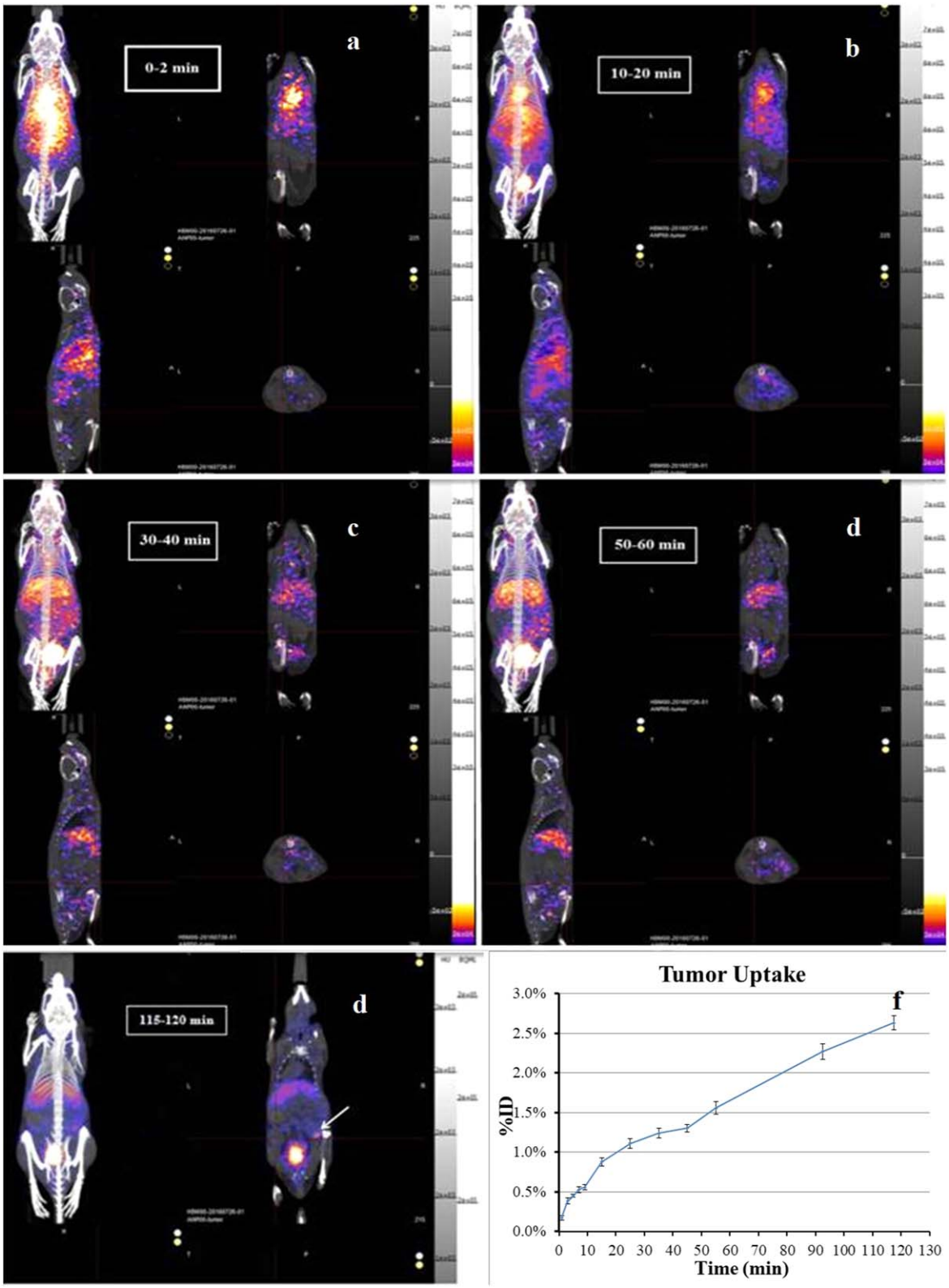

Figure 6. Snapshots of PET-CT images of mice with tumors at the different time intervals (A: 0–2, B: 10–20, C: 30–40, D: 50–60, and E: 115–120 min post-injection and F is the tumor uptake at different time points (decay corrected according to dynamic imaging of mice by analyzed images from nanoScan PET/CT) post-injection (for each panel: maximum intensity projection, upper left; coronal view, upper right; sagittal view, lower left; transverse view, lower right. Color scale: CT: gray to blank; PET: blue to yellow).

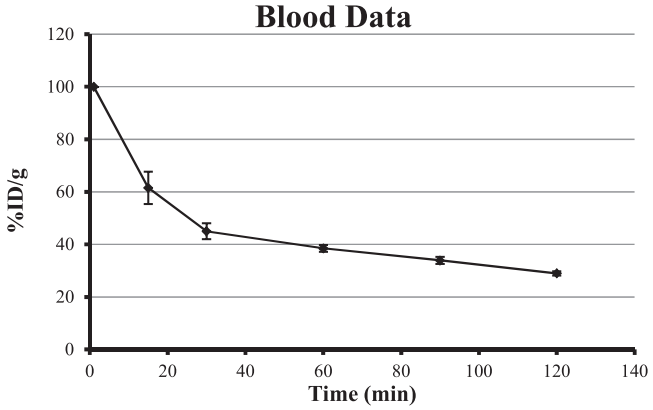

Figure 7. Evaluation of ^{68}Ga-NODA-USPION-BBN blood clearance at different time points. Data are presented as mean ±SD (measurement in triplicate of each sample), with mean values as a percentage of administered activity per gram of blood punction (decay corrected).

Table 3. Biodistribution of ^{68}Ga-NODA-USPION-BBN at different time points. Data are presented as mean ±SD (measurement in triplicate of each sample) %ID/g (decay corrected).

	Time		
Organs	60 min	90 min	120 min
Urine	39.30 ± 2.49	46.39 ± 2.68	33.09 ± 1.45
Liver	9.61 ± 0.83	9.68 ± 0.84	9.10 ± 1.03
Spleen	12.73 ± 1.07	9.33 ± 0.75	8.26 ± 0.74
Lung	20.84 ± 1.76	13.24 ± 0.92	7.03 ± 0.28
Kidney	21.19 ± 1.43	11.58 ± 1.04	9.7 ± 0.52
Blood	39.30 ± 2.49	33.39 ± 2.68	29.09 ± 1.45

ORCID iDs

Afsaneh Lahooti https://orcid.org/0000-0002-7590-8721
Saeed Shanehsazzadeh https://orcid.org/0000-0002-6923-9461
Sophie Laurent https://orcid.org/0000-0002-2589-3250

References

[1] Tabouret-Viaud C, Botsikas D, Delattre B M, Mainta I, Amzalag G, Rager O, Vinh-Hung V, Miralbell R and Ratib O 2015 PET/MR in breast cancer *Semin. Nucl. Med.* **45** 304–21
[2] Pennant M *et al* 2010 A systematic review of positron emission tomography (PET) and positron emission tomography/computed tomography (PET/CT) for the diagnosis of breast cancer recurrence *Health Technol. Assess.* **14** 1–103
[3] Hayat M J, Howlader N, Reichman M E and Edwards B K 2007 Cancer statistics, trends, and multiple primary cancer analyses from the Surveillance, Epidemiology, and End Results (SEER) program *Oncologist* **12** 20–37
[4] Liu Y *et al* 2019 Non-invasive sensitive brain tumor detection using dual-modality bioimaging nanoprobe *Nanotechnology* **30** 275101
[5] Lahooti A, Shanehsazzadeh S and Laurent S 2018 Dual-modality imaging *Iron Oxide Nanoparticles for Biomedical Applications* ed M Mahmoudi and S Laurent (Amsterdam: Elsevier) Ch 7 pp 165–96
[6] Jafari A, Salouti M, Shayesteh S F, Heidari Z, Rajabi A B, Boustani K and Nahardani A 2015 Synthesis and characterization of bombesin-superparamagnetic iron oxide nanoparticles as a targeted contrast agent for imaging of breast cancer using MRI *Nanotechnology* **26** 075101
[7] Xiao L *et al* 2018 Development of a novel drug targeting delivery system for cervical cancer therapy *Nanotechnology* **30** 075604
[8] Poon W, Zhang X, Bekah D, Teodoro J G and Nadeau J L 2015 Targeting B16 tumors *in vivo* with peptide-conjugated gold nanoparticles *Nanotechnology* **26** 285101
[9] Gehrmann M, Stangl S, Foulds G A, Oellinger R, Breuninger S, Rad R, Pockley A G and Multhoff G 2014 Tumor imaging and targeting potential of an Hsp70-derived 14-mer peptide *PLoS One* **9** e105344
[10] Markwalder R and Reubi J C 1999 Gastrin-releasing peptide receptors in the human prostate: relation to neoplastic transformation *Cancer Res.* **59** 1152–9
[11] Richter S, Wuest M, Bergman C N, Krieger S, Rogers B E and Wuest F 2016 Metabolically stabilized (68)Ga-NOTA-bombesin for PET imaging of prostate cancer and influence of protease inhibitor phosphoramidon *Mol. Pharm.* **13** 1347–57
[12] Reubi J C, Korner M, Waser B, Mazzucchelli L and Guillou L 2004 High expression of peptide receptors as a novel target in gastrointestinal stromal tumours *Eur. J. Nucl. Med. Mol.* I **31** 803–10
[13] Sun B, Schally A V and Halmos G 2000 The presence of receptors for bombesin/GRP and mRNA for three receptor subtypes in human ovarian epithelial cancers *Regul. Pept.* **90** 77–84
[14] Lahooti A *et al* 2017 PEGylated superparamagnetic iron oxide nanoparticles labeled with 68Ga as a PET/MRI contrast agent: a biodistribution study *J. Radioanal. Nucl. Ch.* **311** 769–74
[15] Laurent S, Lahooti A, Shanehsazzadeh S and Muller R N 2017 Nano delivery systems *Drug Delivery Systems* (Singapore: World Scientific) Ch 9 pp 277–341
[16] Kukowska-Latallo J F, Candido K A, Cao Z, Nigavekar S S, Majoros I J, Thomas T P, Balogh L P, Khan M K and Baker J R Jr 2005 Nanoparticle targeting of anticancer drug improves therapeutic response in animal model of human epithelial cancer *Cancer Res.* **65** 5317–24
[17] Fang J, Nakamura H and Maeda H 2011 The EPR effect: unique features of tumor blood vessels for drug delivery, factors involved, and limitations and augmentation of the effect *Adv. Drug Deliv. Rev.* **63** 136–51
[18] Gautier J, Allard-Vannier E, Hervé-Aubert K, Soucé M and Chourpa I 2013 Design strategies of hybrid metallic nanoparticles for theragnostic applications *Nanotechnology* **24** 432002
[19] Bridot J L, Stanicki D, Laurent S, Boutry S, Gossuin Y, Leclère P, Lazzaroni R, Vander Elst L and Muller R N 2013 New carboxysilane-coated iron oxide nanoparticles for nonspecific cell labelling *Contrast Media Mol.* I **8** 466–74
[20] Maeda H 2001 The enhanced permeability and retention (EPR) effect in tumor vasculature: the key role of tumor-selective macromolecular drug targeting *Adv. Enzyme Regul.* **41** 189–207
[21] Lee H Y, Li Z, Chen K, Hsu A R, Xu C, Xie J, Sun S and Chen X 2008 PET/MRI dual-modality tumor imaging using arginine-glycine-aspartic (RGD)-conjugated radiolabeled iron oxide nanoparticles *J. Nucl. Med.* **49** 1371–9
[22] Cai W and Chen X 2007 Nanoplatforms for targeted molecular imaging in living subjects *Small* **3** 1840–54

[23] Jimenez-Mancilla N, Ferro-Flores G, Santos-Cuevas C, Ocampo-Garcia B, Luna-Gutierrez M, Azorin-Vega E, Isaac-Olive K, Camacho-Lopez M and Torres-Garcia E 2013 Multifunctional targeted therapy system based on 99 mTc/177Lu-labeled gold nanoparticles-Tat(49-57)-Lys3-bombesin internalized in nuclei of prostate cancer cells *J. Labelled Compd. Rad.* **56** 663–71

[24] Pellico J *et al* 2016 Fast synthesis and bioconjugation of (68) Ga core-doped extremely small iron oxide nanoparticles for PET/MR imaging *Contrast Media Mol.* I **11** 203–10

[25] Varasteh Z *et al* 2013 Synthesis and characterization of a high-affinity NOTA-conjugated bombesin antagonist for GRPR-targeted tumor imaging *Bioconjug. Chem.* **24** 1144–53

[26] Mansi R, Wang X, Forrer F, Kneifel S, Tamma M L, Waser B, Cescato R, Reubi J C and Maecke H R 2009 Evaluation of a 1,4,7,10-tetraazacyclododecane-1,4,7,10-tetraacetic acid-conjugated bombesin-based radioantagonist for the labeling with single-photon emission computed tomography, positron emission tomography, and therapeutic radionuclides *Clin. Cancer Res.* **15** 5240–9

[27] Shanehsazzadeh S, Gruettner C, Lahooti A, Mahmoudi M, Allen B J, Ghavami M, Daha F J and Oghabian M A 2015 Monoclonal antibody conjugated magnetic nanoparticles could target MUC-1-positive cells *in vitro* but not *in vivo* *Contrast Media Mol.* I **10** 225–36

[28] Mahmoudi M, Shokrgozar M A and Behzadi S 2013 Slight temperature changes affect protein affinity and cellular uptake/toxicity of nanoparticles *Nanoscale* **5** 3240–4

[29] Mahmoudi M, Shokrgozar M A, Sardari S, Moghadam M K, Vali H, Laurent S and Stroeve P 2011 Irreversible changes in protein conformation due to interaction with superparamagnetic iron oxide nanoparticles *Nanoscale* **3** 1127–38

[30] Mahmoudi M, Hosseinkhani H, Hosseinkhani M, Boutry S, Simchi A, Journeay W S, Subramani K and Laurent S 2011 Magnetic resonance imaging tracking of stem cells *in vivo* using iron oxide nanoparticles as a tool for the advancement of clinical regenerative medicine *Chem. Rev.* **111** 253–80

[31] Mahmoudi M, Lynch I, Ejtehadi M R, Monopoli M P, Bombelli F B and Laurent S 2011 Protein-nanoparticle interactions: opportunities and challenges *Chem. Rev.* **111** 5610–37

[32] Nosrati S, Shanehsazzadeh S, Yousefnia H, Gholami A, Gruttner C, Jalilian A R, Hosseini R H and Lahooti A 2016 Biodistribution evaluation of 166Ho-DTPA-SPION in normal rats *J Radioanal. Nucl. Ch.* **307** 1559–66

[33] Shanehsazzadeh S *et al* 2016 Development of 177Lu-DTPA-SPIO conjugates for potential use as a dual contrast SPECT/MRI imaging agent *Radiochim. Acta* **104** 337–44

[34] Shanehsazzadeh S, Oghabian M A, Lahooti A, Abdollahi M, Abolghasem Haeri S, Amanlou M, Daha F J and Allen B J 2013 Estimated background doses of [67Ga]-DTPA-USPIO in normal Balb/c mice as a potential therapeutic agent for liver and spleen cancers *Nucl. Med. Commun.* **34** 915–25

[35] Mahmoudi M, Sheibani S, Milani A S, Rezaee F, Gauberti M, Dinarvand R and Vali H 2015 Crucial role of the protein corona for the specific targeting of nanoparticles *Nanomedicine (Lond)* **10** 215–26

[36] Mirshafiee V, Mahmoudi M, Lou K, Cheng J and Kraft M L 2013 Protein corona significantly reduces active targeting yield *Chem. Commun.* **49** 2557–9

[37] Salvati A *et al* 2013 Transferrin-functionalized nanoparticles lose their targeting capabilities when a biomolecule corona adsorbs on the surface *Nat. Nanotechnol.* **8** 137–43

[38] Sun Y *et al* 2016 Preclinical study on GRPR-targeted (68)Ga-probes for PET imaging of prostate cancer *Bioconjug. Chem.* **27** 1857–64

[39] Azhdarzadeh M, Atyabi F, Saei A A, Varnamkhasti B S, Omidi Y, Fateh M, Ghavami M, Shanehsazzadeh S and Dinarvand R 2016 Theranostic MUC-1 aptamer targeted gold coated superparamagnetic iron oxide nanoparticles for magnetic resonance imaging and photothermal therapy of colon cancer *Colloid Surface* B **143** 224–32

[40] Mirsadeghi S, Shanehsazzadeh S, Atyabi F and Dinarvand R 2016 Effect of PEGylated superparamagnetic iron oxide nanoparticles (SPIONs) under magnetic field on amyloid beta fibrillation process *Mater. Sci. Eng. C. Mater. Biol. Appl.* **59** 390–7

[41] Lahooti A, Sarkar S, Laurent S and Shanehsazzadeh S 2016 Dual nano-sized contrast agents in PET/MRI: a systematic review *Contrast Media Mol.* I **11** 428–47

[42] Hajesmaeelzadeh F, Shanehsazzadeh S, Gruttner C, Daha F J and Oghabian M A 2016 Effect of coating thickness of iron oxide nanoparticles on their relaxivity in the MRI *Iran J. Basic Med. Sci.* **19** 166–71

[43] Liu C, Zou B, Rondinone A J and Zhang Z J 2000 Chemical control of superparamagnetic properties of magnesium and cobalt spinel ferrite nanoparticles through atomic level magnetic couplings *J. Am. Chem. Soc.* **122** 6263–7

[44] LaConte L E, Nitin N, Zurkiya O, Caruntu D, O'Connor C J, Hu X and Bao G 2007 Coating thickness of magnetic iron oxide nanoparticles affects R2 relaxivity *J. Magn. Reson. Imaging* **26** 1634–41